Available online at www.sciencedirect.com
SCIENCE DIRECT®
Tectonophysics 416 (2006) 187–207
TECTONOPHYSICS
www.elsevier.com/locate/tecto

An investigation of upper mantle heterogeneity beneath the Archaean and Proterozoic crust of western Canada from Lithoprobe controlled-source seismic experiments

Andrew R. Gorman [a,*], Balázs Németh [b], Ron M. Clowes [c], Zoltan Hajnal [d]

[a] *Department of Geology, University of Otago, PO Box 56, Dunedin 9015, New Zealand*
[b] *PotashCorp, 500-122 1st Avenue South, Saskatoon Canada SK S7K 7G3*
[c] *University of British Columbia, Department of Earth and Ocean Sciences, 6339 Stores Road, Vancouver Canada BC V6T 1Z4*
[d] *University of Saskatchewan, Department of Geological Sciences, 114 Science Place, Saskatoon Canada SK S7N 5E2*

Accepted 28 November 2005
Available online 17 February 2006

Abstract

Observations of upper mantle reflectivity at numerous locations around the world have been linked to the presence of a heterogeneous distribution of rock types within a broad layer of the upper mantle. This phenomenon is observed in wide-angle reflection data from Lithoprobe's Alberta Basement Transect [the SAREX and Deep Probe experiments of 1995] and Trans-Hudson Orogen Transect [the THoRE experiment of 1993]. SAREX and Deep Probe image the Archaean lithosphere of the Hearne and Wyoming Provinces, whereas THoRE images the Archaean and Proterozoic lithosphere of the Trans-Hudson Orogen and neighbouring areas.

Finite-difference synthetic seismograms are used to constrain the position and physical properties of the reflective layer. SAREX/Deep Probe modelling uses a 2-D visco-elastic finite-difference routine; THoRE modelling uses a pseudospectral algorithm. In both cases, the upper mantle is parameterized in terms of two media. One medium is the background matrix; the other is statistically distributed within the first as a series of elliptical bodies. Such a scheme is suitable for modelling: (1) variations in lithology (e.g., a peridotite matrix with eclogite lenses) or (2) variations in rheology (e.g., lenses of increased strain within a less strained background).

The synthetic seismograms show that the properties of heterogeneities in the upper mantle do not change significantly between the two Lithoprobe transects. Beneath the Trans-Hudson Orogen in Saskatchewan, the layer is best modelled to lie at depths between 80 and 150 km. Based on observations from perpendicular profiles, anisotropy of the heterogeneities is inferred. Beneath the Precambrian domains of Alberta, 400 km to the west, upper mantle heterogeneities are modelled to occur between depths of 90 and 140 km. In both cases the heterogeneous bodies within the model have cross-sectional lengths of tens of kilometers, vertical thicknesses less than 1 km, and velocity contrasts from the background of −0.3 to −0.4 km/s. Based on consistency with complementary data and other results, the heterogeneous layer is inferred to be part of the continental lithosphere and may have formed through lateral flow or deformation within the upper mantle.

Keywords: Upper mantle heterogeneity; Western Canada; Finite-difference modelling; Controlled-source seismology

* Corresponding author. Fax: +64 3 479 7527.
E-mail addresses: andrew.gorman@otago.ac.nz (A.R. Gorman), binemeth@potashcorp.com (B. Németh), clowes@eos.ubc.ca (R.M. Clowes), zoltan.hajnal@usask.ca (Z. Hajnal).

0040-1951/$ - see front matter © 2006 Elsevier B.V. All rights reserved.
doi:10.1016/j.tecto.2005.11.023

1. Teleseismic Pn and the Pn coda

Long-range (greater than ~600 km) observations of refractions travelling at upper mantle velocities (8.1–8.3 km/s) are not predicted by most homogeneous or smoothly varying models of the upper mantle. However, seismic energy with these velocities has been observed since the 1960s in earthquake seismograms (Bath, 1967) and is often seen in controlled-source refraction/wide-angle reflection (R/WAR) data sets at offsets as great as 3000 km (Pavlenkova, 1996). This teleseismic Pn phase (Bath, 1966), is distinct from the deeper higher-velocity P phase (Fig. 1). At offset distances beyond 600–800 km, the teleseismic Pn phase generally has a greater amplitude than the P phase that precedes it. R/WAR surveys have recorded the teleseismic Pn phase beneath several different cratonic regions of the Earth including: much of northern Eurasia through the Soviet-era Peaceful Nuclear Explosion (PNE) programme (Egorkin and Pavlenkova, 1981; Egorkin et al., 1987); the Baltic Shield and its margins from the FENNOLORA (Guggisberg and Berthelsen, 1987), EUGENO-S (EUGENO-S Working Group, 1988) and BABEL (BABEL Working Group, 1990, 1993) projects; and North America through such Lithoprobe investigations as SNORE in the Slave and Northern Cordilleran Lithospheric Evolution Transect (Fernandez Viejo et al., 1999). Other experiments have recorded the same phase beneath the southwestern European margin and the south Atlantic Ocean (Pavlenkova, 1996) suggesting that the phenomenon is not restricted to continental lithosphere.

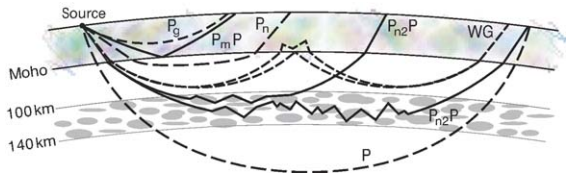

Fig. 1. Schematic summary of lower crust and upper mantle phases (not drawn to scale) identified in controlled-source seismic data sets. Identified phases are represented by raypaths travelling from left to right. Pg—crustal refractions, PmP—reflections from the Moho, Pn—refractions from the uppermost mantle, P—general phase name for refractions from the mantle, WG—whispering gallery phase [any inhomogeneities present in the lower crust add to the complexity of WG (e.g., Morozov et al., 1998; e.g., Nielsen and Thybo, 2003); an example of one such raypath is shown here], Pn_2P—teleseismic Pn that propagates to much greater offsets than Pn; it is similar to Pn except that the near-horizontal portion of the raypath is characterised by multiple reflections and scattering within a distinct layer of heterogeneities in the upper mantle between depths of ~90 and 140 km; two such examples are shown in the figure.

The source of the teleseismic Pn phase can be attributed to either of two scenarios: the whispering gallery phenomenon (e.g., Menke and Richards, 1980; e.g., Morozov et al., 1998; Nielsen and Thybo, 2003; Nielsen et al., 2003), or channelling of energy through multiple reflections and scattering within a heterogeneous region of the upper mantle (e.g., Fuchs and Schulz, 1976; Nielsen et al., 2002; e.g., Perchuc and Thybo, 1996; Ryberg et al., 1995; Thybo and Perchuc, 1997; Tittgemeyer et al., 2000, 1996, 1999) (Fig. 1). A common feature of both of these schemes is a coherent coda of reflected and scattered arrivals that coalesce at far offsets into a discernible teleseismic Pn phase. Interpretations of older R/WAR data sets are limited by the surface sampling interval (often 10s of km), whereas more recent surveys benefit from a station spacing on the order of a kilometer. This enables more subtle waveform characteristics of the upper mantle phases—and in particular the Pn coda at offset distances as low as 200 to 300 km—to be utilised in the interpretation. These upper mantle arrivals are clear on the Lithoprobe R/WAR data sets recorded in the Trans-Hudson Orogen and Alberta Basement transects of western Canada (Clowes et al., 1999).

Whispering gallery models involve multiple reflections of the Pn wave off the underside of the Moho (Fig. 1); the Pn coda is explained by invoking lower crustal heterogeneities (Morozov et al., 1998; Morozov and Smithson, 2000; Nielsen and Thybo, 2003). Morozov (2001) presents strong evidence that the whispering gallery phase is often overlooked in the analysis of R/WAR data sets. However, in specific cases, the modelling of whispering gallery events cannot successfully reproduce either the amplitude characteristics of the teleseismic Pn and Pn coda or the coherent energy in the Pn coda while simultaneously preserving the lower crustal characteristics observed in real data (Nielsen et al., 2003; Tittgemeyer et al., 2000). In the Lithoprobe data sets collected in western Canada (discussed in detail later), the offsets recorded are not optimal for observing the whispering gallery phase and any associated crustal heterogeneities.

Models of upper mantle heterogeneity usually involve the development of a distinct layer of statistically defined reflective bodies bounded above and below by regions that are comparatively transparent seismically. The observation of a large number of spatially continuous seismic reflections within the teleseismic Pn coda implies that heterogeneity in the mantle is the result of thin layering. Ray-trace synthetics indicate that these reflections are near or beyond the critical angle. A variety of modelling methods

previously have been used to further analyse the physical properties of this heterogeneous layer for specific R/WAR studies including the PNE data from the former USSR (e.g., Ryberg et al., 1995; e.g., Tittgemeyer et al., 1996), and the FENNOLORA data from the Baltic Shield (e.g., Perchuc and Thybo, 1996; Thybo and Perchuc, 1997).

Two extreme models for the structure and physical origin of a heterogeneous layer in the uppermost mantle can be considered. One proposes stratification with alternating weak and rigid layers (e.g., Tittgemeyer et al., 1996), perhaps associated with shear-induced anisotropy (Bostock, 1998). The other proposes patchy inhomogeneity as the result of petrological variations (e.g., Ryberg et al., 1996) or low-fraction partial-melt (Thybo and Perchuc, 1997). A likely scenario is to consider a combination of these end-member models (Pavlenkova, 1996; Perchuc and Thybo, 1996). These hybrid interpretations lend credence to the interpretation of additional rheological or petrological discontinuities in the uppermost mantle. Is it possible that the so-called 8° discontinuity (at a depth of approximately 100 km) and Lehmann discontinuity (at a depth of approximately 150 km) represent the bounds of a ubiquitous layer of heterogeneity within the upper mantle (Thybo and Perchuc, 1997)? Can this layer be interpreted as the base of the lithosphere or the top of the asthenosphere?

2. Deep Probe and the Southern Alberta Seismic Experiment

The first of the R/WAR data sets to be discussed was collected as part of the Southern Alberta Seismic Experiment (SAREX) and the Deep Probe Seismic Experiment in 1995 (Fig. 2). SAREX (Clowes et al., 2002) consisted of ten shots, ranging in size from 800 to 2400 kg of explosives, spaced ~50 km apart along a transect in southern Alberta. Deep Probe (Deep Probe Working Group, 1998; Gorman et al., 2002), which targeted greater depths in the upper mantle, comprised ten larger shots, ranging in size from 3000 to 25,000 kg, widely distributed from the Northwest Territories to New Mexico. A maximum of 756 portable seismographs was deployed for the surveys at spacings between 1 and 2 km.

Due to its long offset distances and short spatial sampling interval, the Deep Probe data set is especially well suited to examining the characteristics of the Pn coda and teleseismic Pn. As observed in the Trans-Hudson data and other data sets (e.g., Thybo and Perchuc, 1997), the Deep Probe Pn first arrival data (Fig. 3) show characteristically low amplitudes at offsets less than ~400 km (the exact value varies from one shot record to another). The first arrivals experience an increase in amplitude at offset distances greater than this, coincident with the development of a coherent coda, termed Pn_2P here. The series of events that make up the Pn_2P coda can be identified as a package of intermittently coherent arrivals with apparent velocities between 8.0 and 8.5 km/s which are continuous over tens of kilometers (lying between dashed lines in Fig. 3). Where Pn_2P reflections coincide with dipping mantle reflections (Pf_1P and Pf_2P in Fig. 3), the coda features are clearly seen to have less dip than the upper mantle reflections. The Pn_2P phase has a variable amplitude that is often lower than that of the mantle reflections and can make its interpretation difficult.

3. Trans-Hudson Refraction Experiment

The second dataset to be examined in this paper is the Trans-Hudson Refraction Experiment (THoRE) acquired in north-central Saskatchewan in 1993 (Németh, 1999; Németh et al., in press, 1996; Németh and Hajnal, 1998). The survey is made up of 39 shot points distributed over three major refraction profiles (Fig. 2). A maximum of 505 seismographs, with spacings of 1.0 to 1.5 km, was deployed for each of the profiles. R1 is 725 km long and runs west-to-east on the Phanerozoic cover just south of the outcropping Canadian Shield. R2 is 580 km long and runs south-to-north across the transition from sedimentary-covered platform to exposed Precambrian shield. The parallel profile, R3, is located 200 km west of R2 and is 720 km long. The westernmost shot of THoRE profile R1 was located ~250 km northeast of the northernmost shot of SAREX. The experiment provided data with exceptionally good signal-to-noise ratios—even at large source receiver distances. There is a significant difference in the signal character and penetration depth of shots located in sedimentary and crystalline geological settings. Shots fired in the sedimentary environment generated much stronger and lower frequency signals than those shot in crystalline rocks. Nevertheless, signals generated in the rocks of the Precambrian shield at northern and eastern locations often were recorded with higher signal-to-noise ratio; this can be explained by the higher levels of cultural noise in the southern, more populated parts of the survey area.

Seismic phases propagating in the upper mantle are generally sharp and well defined (Fig. 4). The real surprise of the experiment was the detection of high-quality primary and secondary mantle phases at medium (>300 km) to maximum offsets. On some records the Pn phase is very complex at offsets close to the PmP reflection, giving evidence of substantial structures near

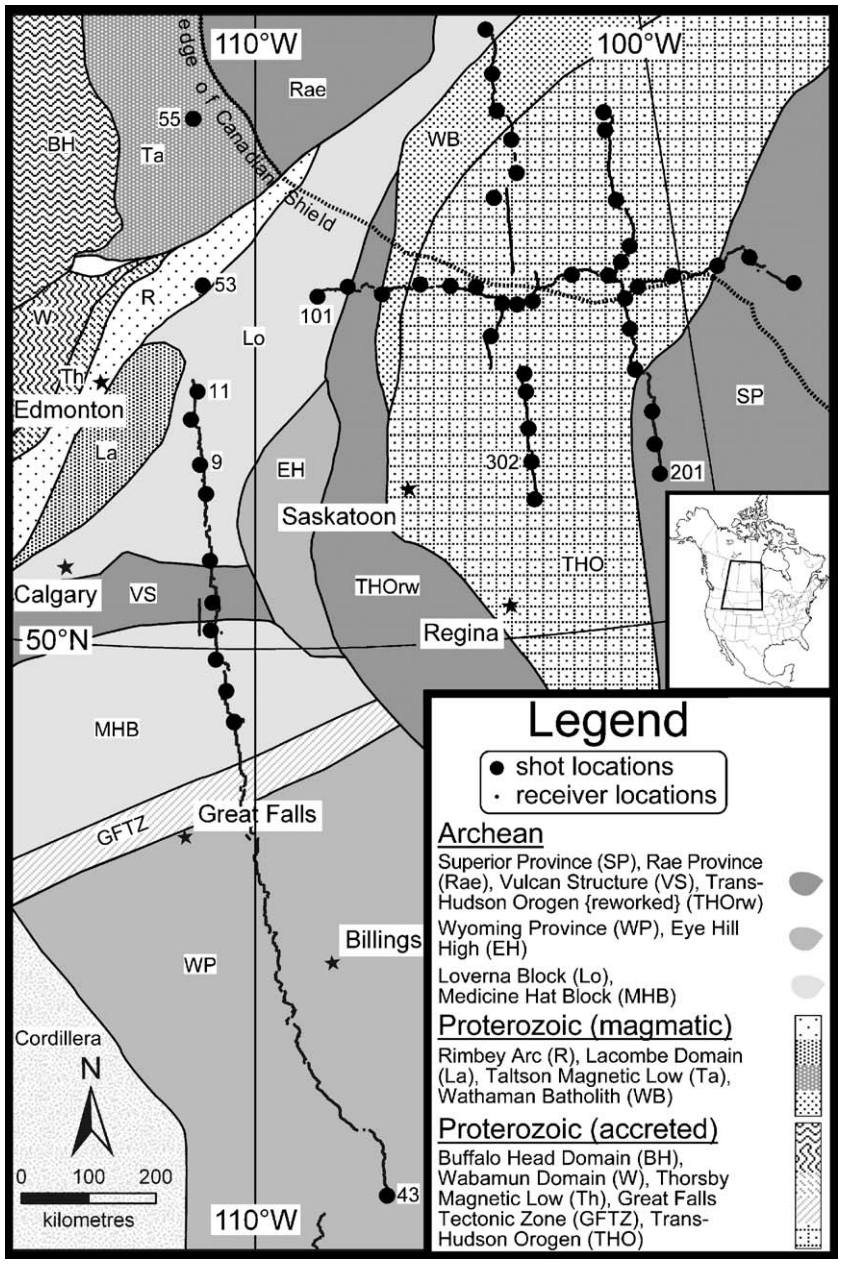

Fig. 2. Location map showing the Southern Alberta Refraction Experiment (SAREX), Deep Probe, and Trans-Hudson Refraction Experiment (ThoRE) locations in western North America. Small circles (overlapping to form a line) are seismograph stations occupied for the active source experiments. Major crustal domains are indicated (e.g., Villeneuve et al., 1993).

the base of the crust. On records with offsets larger than 300 km, a Pn_2P band of secondary mantle phases within the Pn coda is evident (Fig. 4).

4. Estimating velocity structures

Refraction seismic data traditionally have been interpreted by modelling the traveltimes of observed seismic phases using a method such as ray theory (Cerveny et al., 1977). These methods can quickly compute the arrival time and amplitude of specific phases (PmP, Pn, etc.) for earth models, but their application is limited to arrivals that are computable within the theoretical considerations of the technique (Cerveny et al., 1977; Chapman, 1985). During this modelling process, theoretical seismic responses of

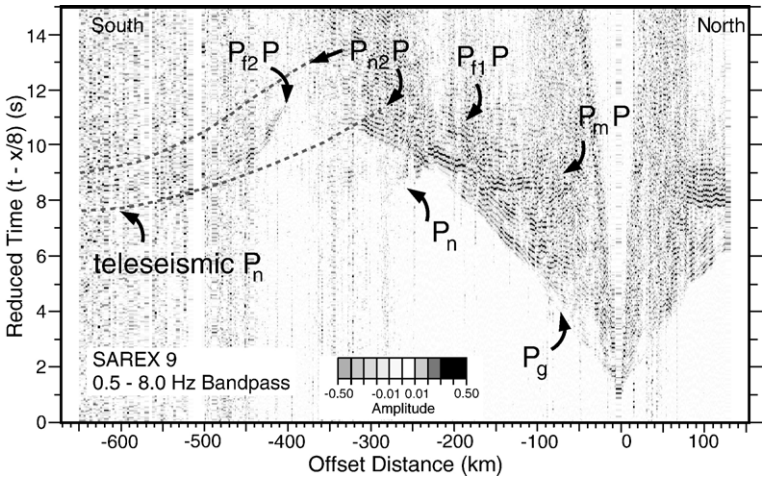

Fig. 3. Seismic record SAREX 9 showing typical phases observed in southern Alberta. Teleseismic Pn and Pn coda features are highlighted. Coherent Pn_2P events associated with upper mantle heterogeneities lie between dashed grey lines. $P_{f1}P$ and $P_{f2}P$ are distinct reflections that are modelled to be the result of dipping reflectors in the upper mantle (see Fig. 5). Data are trace normalised and plotted in variable density as indicated; synthetic calculations of SAREX/Deep Probe data presented here are plotted in a similar fashion.

velocity models are compared to the observed arrivals. The velocity models are then modified using inversion algorithms until a satisfactory fit between the observation and the predicted arrivals is achieved. The ray-theoretical traveltime inversion algorithm of Zelt and Smith (1992) has been utilised to constrain velocity models for the crust and upper mantle of the Trans-Hudson Orogen (Németh et al., in press, 1996; Németh and Hajnal, 1998) and Alberta Basement (Clowes et al., 2002; Gorman et al., 2002). These models are modified here to create synthetic seismograms corresponding to recorded shots. For the SAREX/Deep Probe data, a visco-elastic finite-difference method (Levander, 1989; Robertsson et al., 1994) has been used. For THoRE, a pseudo-spectral method (Gazdag, 1982; Kosloff and Baysal, 1982) was used. In both cases, the seismic source was approximated as a Ricker wavelet with a central frequency ranging between 1.75 and 5.5 Hz.

Synthetic seismic problems with complex velocity structures and/or complex stratigraphy characterised by irregular interfaces can be solved efficiently and accurately by numerical methods such as finite differences (Aki and Richards, 1980; Kelly et al., 1976). Classic finite difference methods solve the wave equation by approximating the time and spatial derivative terms of the equation numerically on a grid. The long recording time and great offset range of an R/WAR survey require higher order approximation of the derivatives and finer grid spacing than exploration type models to avoid the accumulation of computational noise (Alford et al., 1974). The visco-elastic finite difference routine utilised for the Alberta Basement transect (Robertsson et al., 1994) made use of initial P-wave velocity models. Models of S-wave velocity, density and dispersion were established using simple relationships (Table 1). The method is accurate to fourth order in space and to second order in time.

In order to reduce the time required to model shot records from the Trans-Hudson Orogen transect, an efficient numerical solver was developed by Németh (1999). To further reduce computational time, only the acoustic wave equation was considered. This is justified by the observation of high apparent velocity and particle motion of the Pn_2P phase suggesting that it is purely compressional. Frequency dependent attenuation and dispersion were not included in the computation at this stage either. Since the modelled phase has a narrow frequency spectrum and the seismic attenuation in the utilised frequency range is low within the mantle and the crust, it is unlikely that dispersion would affect the results.

In the sections that follow, a series of finite-difference models are presented that investigate properties of a heterogeneous upper mantle specific to the Trans-Hudson Orogen and Alberta Basement Transects in western Canada. To construct the models, ray tracing was used to obtain a first-order estimation of the depth range and velocity of the zone where these arrivals originated. In the case of the THoRE data, the depth of this investigation is greater than the maximum depth of Pn penetration; therefore, no velocity information was available from the refraction data. Consequently, velocity values from teleseismic studies were incorporated to extend the velocity models downward. Later

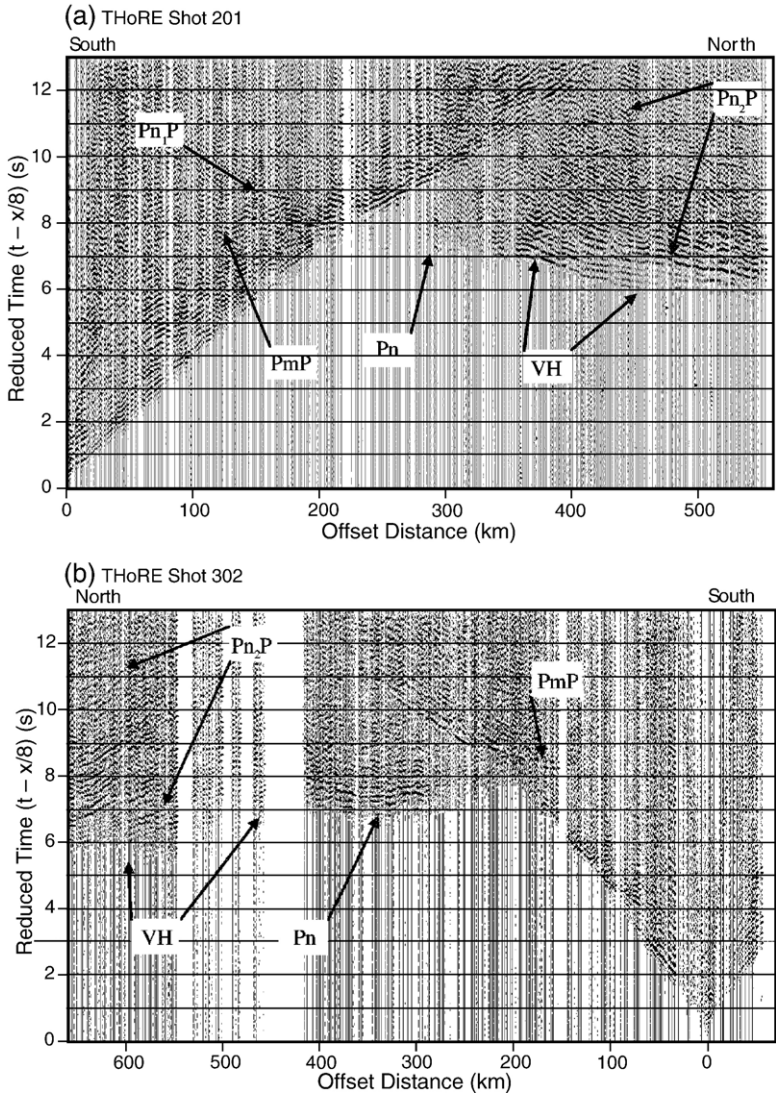

Fig. 4. Seismic records (a) ThoRE 201 and (b) ThoRE 302 showing typical upper mantle phases observed in data from the Trans-Hudson Refraction Experiment. Traces are bandpass filtered from 2.5 to 7.5 Hz. Phase identifications: PmP—reflections from the Moho, Pn—refracted arrivals from the uppermost mantle, Pn_1P—reflected arrival from the upper mantle, Pn_2P—reflected arrivals from deeper in the mantle (subject of this paper). VH marks arrivals with unusually high apparent velocity. The Pn_2P phase includes all the secondary events observed beyond offsets of 300 km. Data are trace normalised and plotted in variable area; synthetic calculations of THoRE data presented here are plotted in a similar fashion.

these velocity values were adjusted according to the demands of the inversion process.

Ray-trace modelling of a single reflection phase in a set of arrivals could lead to significant errors in depth and velocity estimation (Levander and Holliger, 1992). To avoid such an error, the top and bottom envelope of the Pn_2P events were picked, and inverted as the upper and lower boundary of the reflective mantle zone. This technique supplies the correct depth, average velocity and velocity gradient of the heterogeneous zone; the finite-difference modelling provides information about the small-scale variations.

The velocity model for the finite difference algorithms is specified as a grid. The grid spacing and size are chosen according to the desired maximum signal wavelength: typically in the range of 350 m. Once the initial velocity grid has been established from the results of ray-trace modelling, velocity inhomogeneities are added to the model in the form of ellipses. A similar modelling method was used by Reston (1987) to compute lower crustal reflectivity created by extension. His work demonstrated that reflectivity of the lower crust must be created by spatial interfaces with sizes or topography smaller than the diameter of the first Fresnel

Table 1
Viscoelastic parameter relationships used for input ranges of compressional velocities (v_p)

V_p range (m/s)	V_p/V_s	Density (kg/m^3)	Q_p	Q_s
3600–4200	1.73	2700	50	10
4200–5000	1.73	2700	100	25
5000–6500	1.73	2750	400	200
6500–8100	1.78	3000	400	200
8100–9400	1.81	3380	2000	1000

zone to match the typical observations. For our upper mantle investigation, synthetic seismograms are produced to match observed reflectivity patterns (including observations of trace-to-trace coherence, amplitude and frequency.) The real structures are probably more complex and irregular (e.g., Crossley and Jensen, 1989; Levander et al., 1994) than the elliptical bodies used here. However, this geometrically simple form appears to be sufficient for first order modelling approximations. Although formally defined statistical models of the upper mantle structures are possible (e.g., Allègre and Turcotte, 1986; Meibom and Anderson, 2003), the elliptical body approach facilitates the ad hoc manipulation of model parameters such as the size and spatial distribution of inhomogeneities.

The definition of the upper mantle heterogeneous layer includes: the depth range over which the ellipses are added, the horizontal and vertical distribution of the ellipses, and the parameters of the ellipses (width, thickness, velocity perturbation, and tilt angle). These parameters are treated as random variables with normal distributions. Consequently, the mean value and standard deviation of these variables were specified as parameters of the model. This approach permits the easy creation of complicated 2-D velocity structures. For example, a tilted and layered structural block can be generated by "stretching" the ellipses along their horizontal axes and then rotating them by a specified angle. Typically, the spatial dimensions of the ellipses were only a few times larger than the grid spacing of the velocity model, which caused the boundaries of the structures to be coarse. This "graininess" introduces additional structural variations into the model. Tables 2 and 3 summarise the parameters used for models presented in this paper.

These 2-D structures were inserted into the velocity models to create a reflective mantle. Synthetic responses were compared to the observations. The primary goal of these tests was to investigate the effect of structural two-dimensionality on the character of the Pn_2P phase, and to estimate the parameters of the "real" inhomogeneities.

5. Alberta basement

In the Deep Probe/SAREX data, the Pn_2P phase is observed as a 2- to 4-s-long sequence of spatially semi-continuous arrivals within the coda of the Pn phase (Fig. 3). Coherent arrivals within this coda are observed to be spatially continuous over 5–50 km. The dominant frequency of the signal is in the range of 3.5–6.0 Hz. At offsets of around 325 km, the onset of the Pn_2P is marked by an apparent velocity near 10 km/s. At greater distances (500 to 650 km) it flattens into the teleseismic Pn refraction with an apparent velocity near 8.1 km/s.

Table 2
Model parameters varied for the Deep Probe/SAREX profile

Model/ synthetic (figure numbers)	x (km)	z (km)	Central frequency (Hz)	v (km/s at 100 km)	Areal extent of anomalies (%)
5/6b	24	0.48	1.75	8.38	30
5/6d	24	0.48	3.25	8.38	30
7a/7b	48	0.96	3.25	8.38	20
7c/7d	36	0.72	3.25	8.38	20
7c/8b	36	0.72	3.25	8.38	20

The first column indicates the figures where the model and corresponding synthetic are found. x: horizontal dimension (standard deviation, $\sigma = 0.12$ km in all cases), z: vertical dimension ($\sigma = 0.12$ km in all cases), v: background velocity at a depth of 100 km ($\sigma = 0.05$ km/s in all cases). The gradient of the background velocity is specified as 0.0083 km/s/km in the upper mantle. The approximate areal extent of anomalous bodies within the layer of heterogeneity is indicated.

Table 3
Model parameters varied for the Trans-Hudson Refraction Experiment profiles

Model (figure)	Line	x (km)	Std (x) (km)	z (km)	Std (z) (km)	v (km/s)	Areal extent of anomalies (%)
11a	R2	20	7.5	0.2	0.4	8.0	20
11b	R2	20	7.5	0.2	0.4	8.3	20
11c	R2	20	7.5	0.2	0.4	8.5	20
11d	R2	20	7.5	0.2	0.4	8.7	20
12a	R2	40	7.5	0.2	0.4	8.0	30
12b	R2	10	2.5	0.2	0.4	8.0	8
12c	R2	5	1	0.2	0.4	8.0	4
12d	R2	2.5	1	0.2	0.4	8.0	2
13a	R1	5	1	0.2	0.4	8.0	5
13b	R1	3.5	1	0.2	0.4	8.0	3
13c	R1	1.5	0.2	20	1	8.0	20

x: horizontal dimension (standard deviation, σ as indicated), z: vertical dimension (σ as indicated), v: average velocity at a depth of 50 km ($\sigma = 0.03$ km/s in all cases). The gradient of the background velocity is ~0.004 km/s/km in the upper mantle. The approximate areal extent of anomalous bodies within the layer of heterogeneity is indicated.

The synthetic seismograms presented here are based on modifications to the starting model discussed previously. A layer of statistically defined elliptical bodies has been added between depths of 90 and 140 km. The depth extent of this heterogeneous layer was constrained by an ad hoc iterative modelling procedure; several different combinations of upper and lower bounds were modelled to find a match for the distribution of coherent events in the Pn coda (Gorman, 2000). An example is seen in Fig. 5.

Two finite-difference synthetic seismograms corresponding to shot record SAREX 9 (Fig. 3) have been produced using this first model, one with a central frequency of 1.75 Hz (Fig. 6b) and the other with a central frequency of 3.25 Hz (Fig. 6d; Table 2). These can be compared with the synthetic seismograms from the standard model with a transparent upper mantle (Fig. 6a and c). The comparison is especially useful for identifying features related to the upper mantle dipping reflector as opposed to specific features of the Pn coda. In the first synthetic seismogram produced using this technique (Fig. 6b) that had a central frequency of 1.75 Hz, it is apparent that the layer of elliptical anomalies was observed as an effective medium by the examining wave field. With a central frequency of 1.75 Hz and velocities of ~8.4 km/s, the dominant wavelength in the data at the depth of the upper mantle heterogeneous layer is ~4.8 km, a length considerably greater than the thickness of the ellipses modelled. Continuous upper and lower reflections (labelled A and B, respectively, in Fig. 6b), marking the top and bottom of the zone of ellipses are clearly seen; reflections within the Pn coda are also continuous over long offset ranges. This 'continuous' coda pattern is a result of the effective medium characteristics of the system and is not representative of what is seen in the real data (Fig. 3) that shows intermittently continuous reflections with a much shorter length scale. As a result, the central frequency of the source wavelet was increased to 3.25 Hz to reduce the effective medium characteristics observed in the lower frequency synthetic data. The resulting, higher frequency synthetic seismogram is a closer match to the real data, although it can be argued that the length over which events remain coherent in the Pn coda is shorter than observed in the real data. In this case, though, the short length scale is due to the dimensions of the ellipses used in the model rather than the frequencies used to model them.

Two additional models were subsequently developed to further constrain the ellipse dimensions and distributions within the heterogeneous layer (see Table 2). In the first of these models (Fig. 7a), the size of the ellipses was doubled: to 48 km long by ~1.0 km thick. This resulted in a more coherent Pn coda (Fig. 7b). Reflections within the coda are observed to be coherent over as much as 60 km, longer than that observed in the real data (Fig. 3). This suggests that the ellipse dimensions in this case are too large. In addition, the quantity of coherent events within the coda in the synthetic data is observed to be lower than in the real

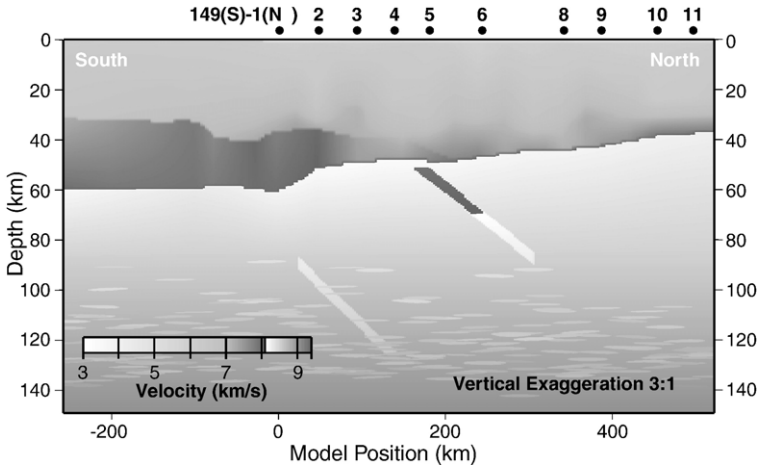

Fig. 5. A P-wave velocity model typical of those used for the finite-difference modelling of the lithosphere of southern Alberta. The basic structure of the model is determined by earlier ray-theoretical travel-time modelling. Significant features included in this modelling include two dipping reflectors in the uppermost mantle (Gorman et al., 2002). Heterogeneity in the upper mantle is added by the addition of stochastically defined elliptical bodies. In this example, elliptical bodies ($x=24\pm0.012$ km, $z=0.48\pm0.012$ km) are inserted between depths of 90 and 140 km. Shot point locations are indicated by numbered dots along the top of the figure. Note the change in the velocity grey scale at 8.1 km/s; this causes the upper half of the dipping reflector at 200 km distance to show as two distinct shades.

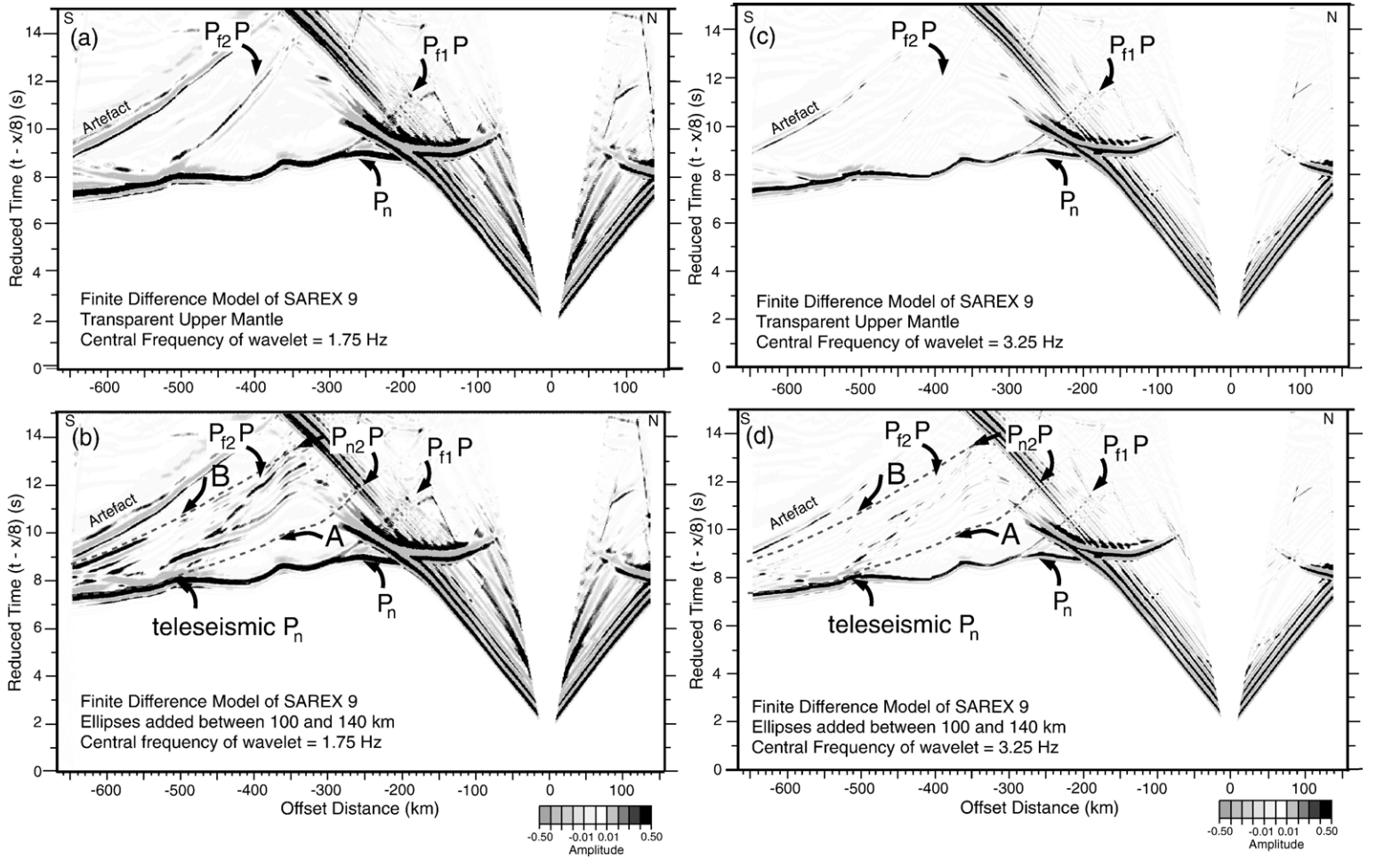

Fig. 6. Comparison of (a) a transparent upper mantle to (b) a mantle with coarse elliptical anomalies between 90 and 140 km with a central frequency of 1.75 Hz. The same models are run in (c) and (d) with a higher frequency wavelet (central frequency = 3.25 Hz). Coherent Pn_2P events associated with upper mantle heterogeneities lie between the grey dashed lines labelled A and B in (b) and (d).

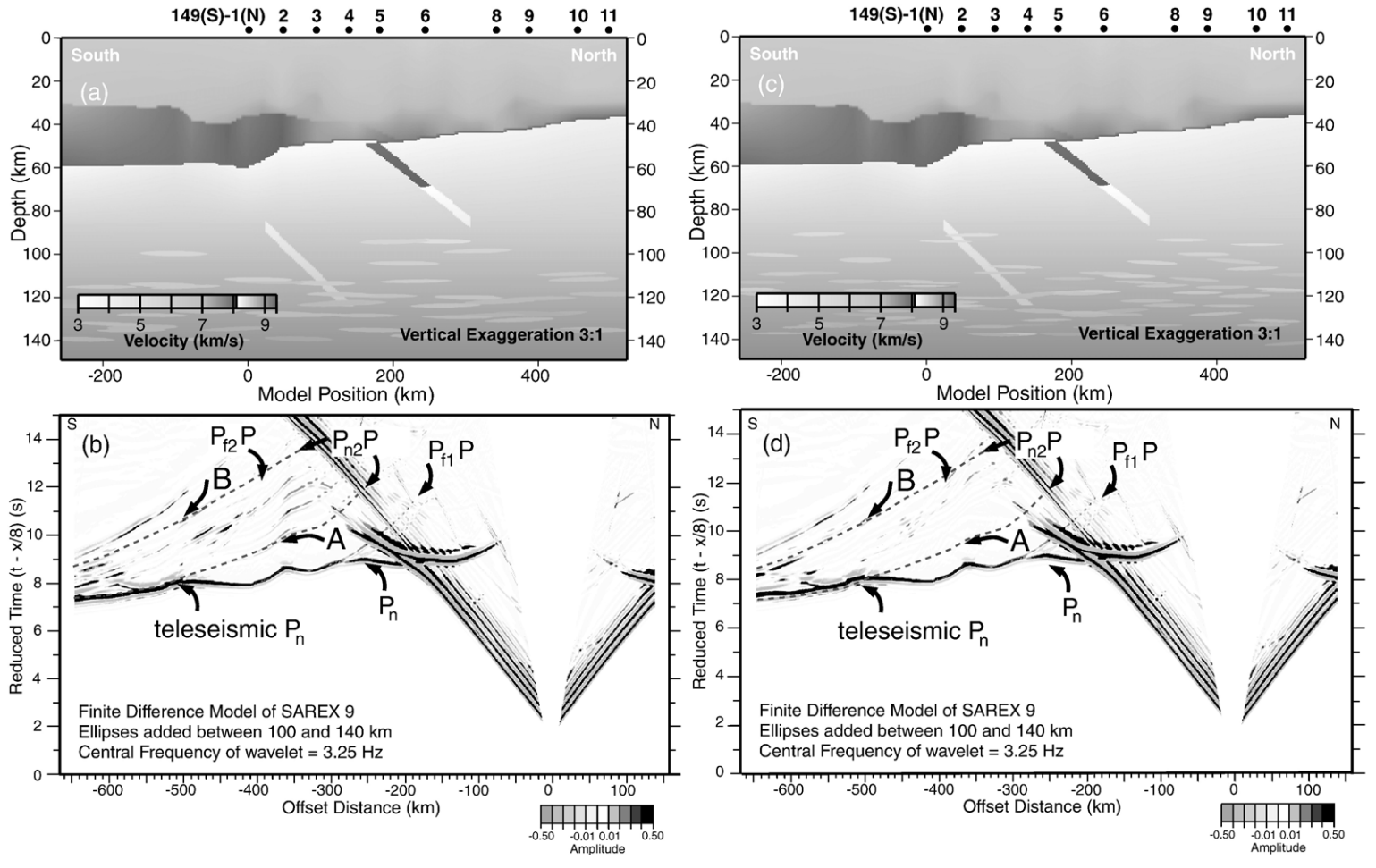

Fig. 7. Comparison of wide (48±0.12 km), thick (0.96±0.12 km) and scarce (1 per 24 km vertical and 1 per 24 km horizontal) elliptical bodies in the upper mantle (parts a and b) to elliptical bodies that are less wide (36±0.12 km), narrower (0.72±0.12 km) and more frequent (1 per 18 km in both vertical and horizontal directions; parts c and d) The latter example better matches the real seismic data.

data suggesting that the density of elliptical bodies in the model is too low. (Note that ellipse distribution parameters are included in the figure captions for each model.) Interference between the upper mantle dipping reflection ($P_{f2}P$) and coherent events in the coda is apparent in both the real data and the synthetic examples. This aspect of the models has not been investigated further.

The middle ground was struck in the final SAREX model with ellipse lengths of 36 km and thicknesses of 0.72 km (Fig. 7c). The density of intermittent coda events seen in the resulting synthetic seismogram (Fig. 7d) matches well with the real data, and the modelled and observed length scales of coherent events in the coda (10–30 km in offset length) also appear to be a fairly close match.

The modelling performed here has partially constrained the dimensions and distribution density of heterogeneous bodies within the proposed upper mantle wave guide (36 by 0.72 km ellipses, with one ellipse per 324 km^2 on average.) The accuracy of these statistical parameters (especially the width of elliptical bodies) is affected by the wavelengths of the real and modelled seismic waves. Several parameters, such as ellipse orientation and velocity contrasts within the heterogeneous bodies have not been evaluated in this limited investigation. For example, in the current models, the inserted ellipses are assumed to be horizontally oriented; inclined elliptical bodies could be representative of a particular method of emplacement or post-emplacement alteration.

The previous models and the synthetic seismograms generated from them have examined the Pn phase and its associated coda at offsets less than 650 km. In order to investigate the seismic character at longer offset distances, the input model was expanded to the dimensions of Deep Probe profile 55 (Fig. 8a). The bottom of the model was increased to 200 km and the length increased to almost 1400 km. The preferred model from the SAREX tests (Fig. 7c) is recast with the dimensions of the Deep Probe shot record.

Comparing the real data for Deep Probe 55 (Fig. 8a) to the synthetic generated for this shot (Fig. 8b) reveals some enlightening features. In the real data, the same general upper mantle features observed in the data from SAREX shot 9 (Fig. 3) are identified. As was seen in the SAREX data, a Pn coda envelope comprised of intermittently coherent events with length scales in the order of 10–30 km and apparent velocities between 8.0 and 8.5 km/s can be identified. The two upper mantle dipping reflections, $P_{f1}P$ and $P_{f2}P$, are identified, both of which crosscut the Pn coda envelope. The formation of the teleseismic Pn by the convergence of Pn coda events into a narrow band, is clearly identified in the data, especially at offset distances greater than 750 km.

The most important result of this finite difference model is that the teleseismic Pn phase observed in the synthetic seismogram (Fig. 8b) propagates with characteristics similar to those seen in the real data. The modelled Pn coda is also seen to occur at the anticipated position, based on the modelling of SAREX shot 9. However, the distribution of reflectivity within the coda has a different character than that seen in the real data, especially in the offset range between 480 and 850 km. This suggests that the model, as constructed based on the modelling of the SAREX data is not completely satisfactory for the farther offset distances seen in the Deep Probe data set. Therefore, the position of the upper mantle heterogeneous layer (between depths of 90 and 140 km) can be confirmed for both the shot positions modelled here, but the exact nature of the heterogeneities within this layer is not completely understood.

The modelled amplitudes of the Pn_2P phase as compared with deeper mantle phases are the reverse of what is seen in the real data. In the real data example (Fig. 8a), the Pn_2P and teleseismic Pn have a greater amplitude than the Pn or body wave P. These amplitudes have not been accurately modelled. 1-D reflectivity modelling of the teleseismic Pn phase (Tittgemeyer et al., 1996) indicates that several criteria control the relative amplitudes of these phases. These criteria include: (i) the distribution of hypothesised scattering bodies of various sizes within the upper mantle, (ii) the physical nature (e.g., impedance contrast, anisotropic properties) of these scattering bodies, and (iii) the background velocity gradient. The first two criteria have been partially investigated for the SAREX example, and the third criterion is controlled by the picks made in the real data for the body wave P phase; possible error in these picks has not been considered in the finite difference modelling. These models have been successful in exploring some of the geometric controls on the seismic response of the uppermost mantle, but clearly, an enhanced and extensive modelling program that examines all possible geometries and visco-elastic properties for the hypothesised scattering bodies should result in a better model for Pn_2P and teleseismic Pn.

6. Trans-Hudson Orogen

The THoRE and SAREX/Deep Probe profiles, located ~500 km apart, have a remarkably similar upper mantle seismic character. In the THoRE data, the Pn_2P phase is observed as a 3- to 6-s-long sequence of

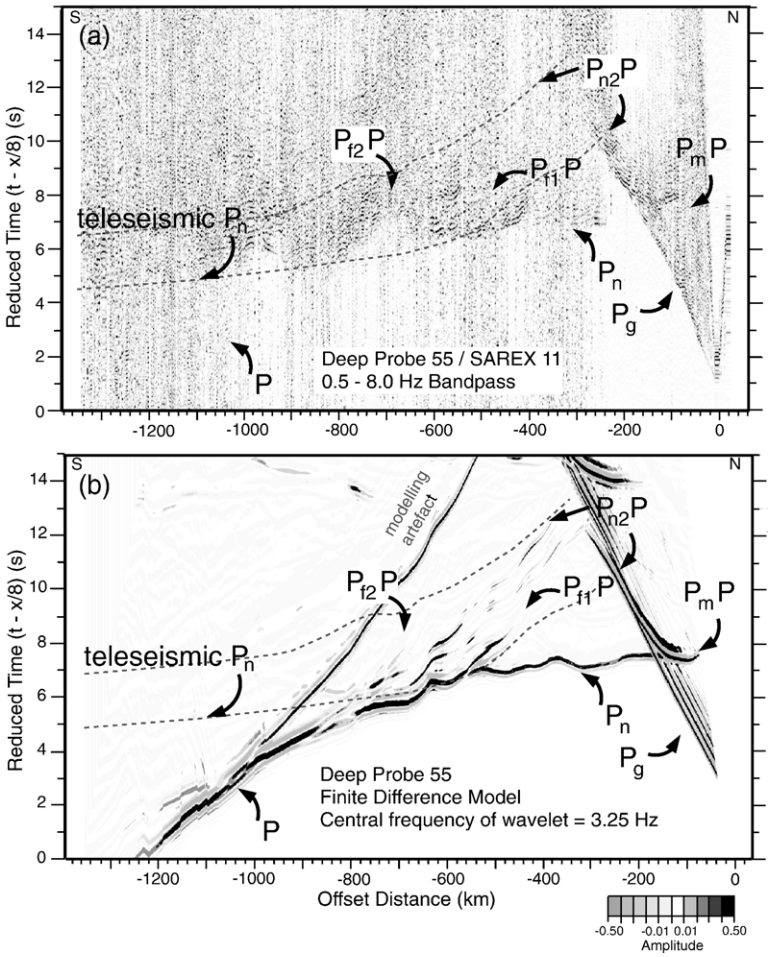

Fig. 8. Comparison of (a) real and (b) synthetic data for seismic record Deep Probe 55 with offsets up to 1350 km. Pn_2P events associated with upper mantle heterogeneity lie between grey dashed lines. Ellipses defined as in Fig. 7(c) and (d). Note that the relative amplitude of teleseismic Pn and P phases do not match; this is partly the result of the background elastic parameters (e.g., the choice of crustal Q may be too high, see Table 1) rather than a direct result of the introduction of upper mantle heterogeneity.

spatially semi-continuous arrivals with variable move-out (e.g., Fig. 4). Some arrivals within this wave coda can be traced spatially over 10–20 km but the typical spatial extent of the arrivals is around 5–7 km. The dominant frequency of this signal is in the range of 3.5–6.0 Hz. Amplitudes near the onset of the coda, after the Pn phase, are the largest and they decrease with time. The end of the wave coda is imaged as a gradual disappearance of coherent energy. At offsets of around 300 km, the onset of the Pn_2P has an apparent velocity near 10 km/s. At greater distances (600 to 750 km) it flattens into the weak Pn refraction with an apparent velocity near 8.3 km/s.

There is a significant difference in the strength and continuity of the Pn_2P event between the recordings of line R1 (oriented east–west) and the two other lines (oriented north–south) (Fig. 9). Along the profile R1 (Fig. 10), seismic sources with the largest charge size failed to generate as continuous and large amplitude Pn_2P events as the smaller shots of R2 and R3 (Fig. 4). Since the crustal and other mantle arrivals have a comparable character along the three profiles, orientation-dependent structural variations are inferred as the most likely cause of the inconsistency in the nature of the Pn_2P.

Far offset, three-component observations at the north end of R3 reveal that the particle movement of the Pn_2P is restricted to the inline direction. This property and the high apparent velocity of the phase at large offsets suggest that these signals are generated at deeper mantle levels, most likely in a highly reflective mantle zone, and not within the crust. To test this hypothesis, synthetic seismic sections were computed for different mantle models and compared to the observations.

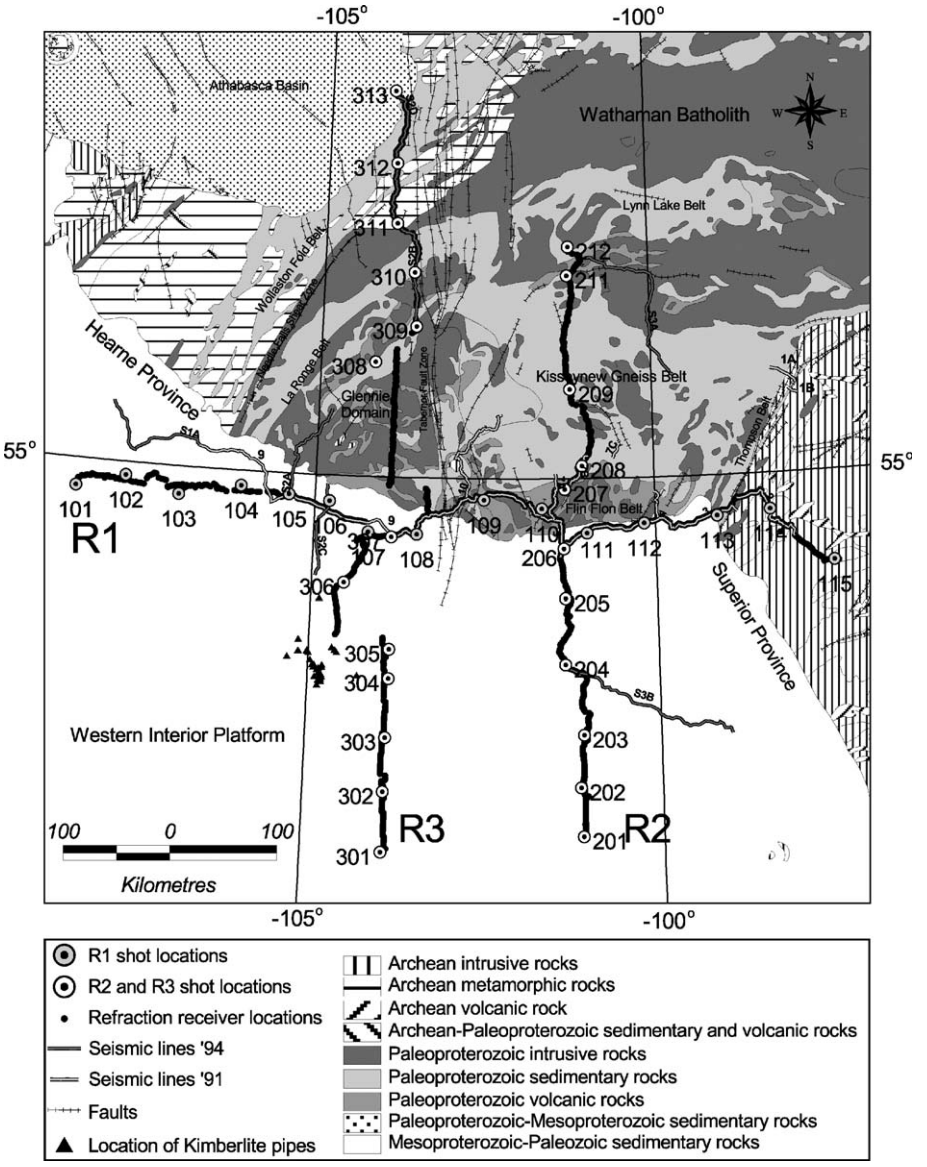

Fig. 9. Location map of THoRE 1993 showing known geological domains on the Canadian Shield.

Figs. 11 and 12 summarise the modelling of shot record THoRE 201 (Fig. 4a) which is representative of the north–south oriented data (profiles R2 and R3). The heterogeneous mantle zone starts at a depth of ~80 km and extends to a depth around 150–160 km on all profiles. Parameters used for the construction of the models are listed in Table 3. The uppermost mantle in the starting model shows significant variation along the profile. Perhaps most apparent is a high-velocity zone extending for ~100 km between kilometers 300 and 400 on profile R2. Németh et al. (2005) describe and discuss this uppermost mantle velocity variation. Source and receiver parameters for the models were chosen to be similar to the ones used during data acquisition. Receivers were located on the surface at every km. The depth of the source was set to 100 m. The source signal was approximated using a Ricker wavelet with 7 Hz maximum and 5.5 Hz peak frequency.

The average velocity of the inclusions was investigated first by modifying the velocity between 8.0 and 8.7 km/s (Fig. 11). Models with velocity contrasts in the range of 0.4 to 0.3 km/s (Fig. 11a and d) created a Pn_2P phase that matched the observations most closely. Models with smaller velocity variation (Fig. 11b and c) do not have enough velocity contrast to create significant Pn_2P phase. Modelling within the offset

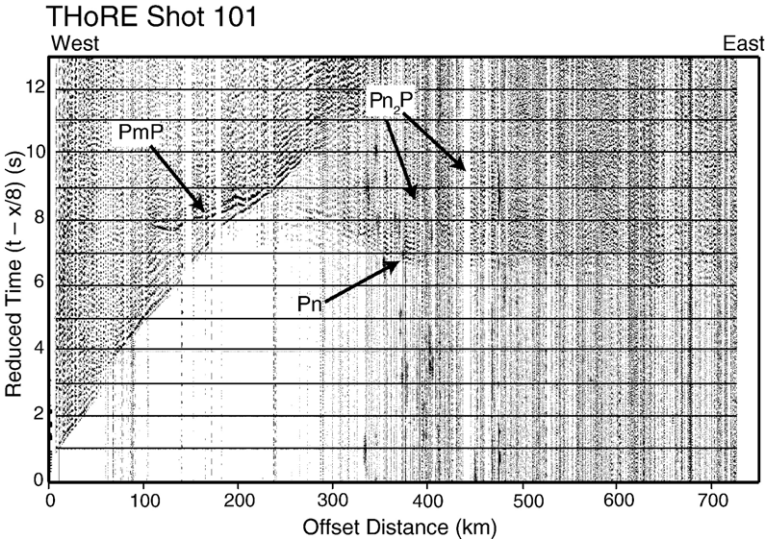

Fig. 10. Seismic record THoRE 101 (oriented west–east) showing typical upper mantle phases. Traces are bandpass filtered from 2.5 to 7.5 Hz. Phase identifications: PmP—reflections from the Moho, Pn—refracted arrivals from the uppermost mantle, Pn_2P—reflected arrivals from deeper in the mantle. The Pn_2P phase includes all the secondary events observed beyond an offset of 300 km.

range shown cannot adequately differentiate heterogeneous bodies with a negative velocity contrast from those with a positive velocity contrast, but longer offset models can do so (see below). A negative velocity contrast with respect to the background velocity is supported by the growing set of teleseismic datasets from cratonic regions that show an overall decline in velocity over a similar depth range (e.g., Frederiksen et al., 2004).

The average width of the structures was modified in the range of 40 to 2.5 km (Fig. 12). As the horizontal length of the inhomogeneities is decreased (Fig. 12a to Fig. 12d), the events within the Pn_2P phase become less coherent and their amplitude decreases, also. Heterogeneous bodies with horizontal dimensions between 20 (Fig. 11a) and 40 km (Fig. 12a) match the observations most closely.

As previously mentioned, the seismic character of the Pn_2P phase is markedly different on east–west profile R1 (Fig. 10) from that seen on the north–south oriented R2 and R3 profiles (Fig. 4). Heterogeneous bodies with average horizontal dimensions between 5.0 (Fig. 13a) and 2.5 km (Fig. 13b) match the observations most closely in this case. This suggests a strongly anisotropic nature for the heterogeneous layer. In three dimensions, individual heterogeneities would resemble cigar-shaped bodies. No significant Pn_2P phase was generated in the synthetic seismogram when the average orientation of the major axes of the ellipses was vertical (Fig. 13c). This indicates that the phase is mainly determined by the horizontal length of the inhomogeneities.

7. Nature of Pn_2P at teleseismic distances

The maximum offset of the refraction records in the Trans-Hudson data set is limited to 750 km. However, to study the behaviour of the Pn_2P phase beyond this offset, two finite difference seismograms with offsets up to 2500 km distance were computed (Fig. 14) from models similar to those shown in Fig. 11. Seismic velocities in the mantle were selected to be similar to the observations, increasing from 8.2 km/s at the base of the crust to 8.5 km/s at a depth of 160 km. Fig. 14a was prepared by including elliptical structures with an average velocity of 8.6 km/s, the same as in Fig. 11d. In Fig. 14b, the average velocity of the structures was set to 8.0 km/s, similar to Fig. 11a.

The Pn phase is visible on both sections with an identical apparent velocity of 8.2 km/s. Also, the Pn_2P phase has similar moveout and character up to offsets of ~1000 km on both sections. However, beyond 1000 km the appearance of Pn_2P deviates. For the model with high-velocity inclusions (Fig. 14a), at around 1200 km offset, the Pn_2P phase becomes the first arrival in front of the Pn phase with an apparent velocity around 8.5 km/s. In the model with low-velocity lenses, the Pn_2P phase stays behind the Pn.

On both records at offsets less than 1000 km, the Pn_2P is imaged as a package of semi-continuous arrivals with variable apparent velocity and relatively well-defined onset and termination. Beyond 1500 km, however, the Pn_2P becomes an approximately 6-s-long wave-train consisting of many weak, parallel arrivals without a sharp

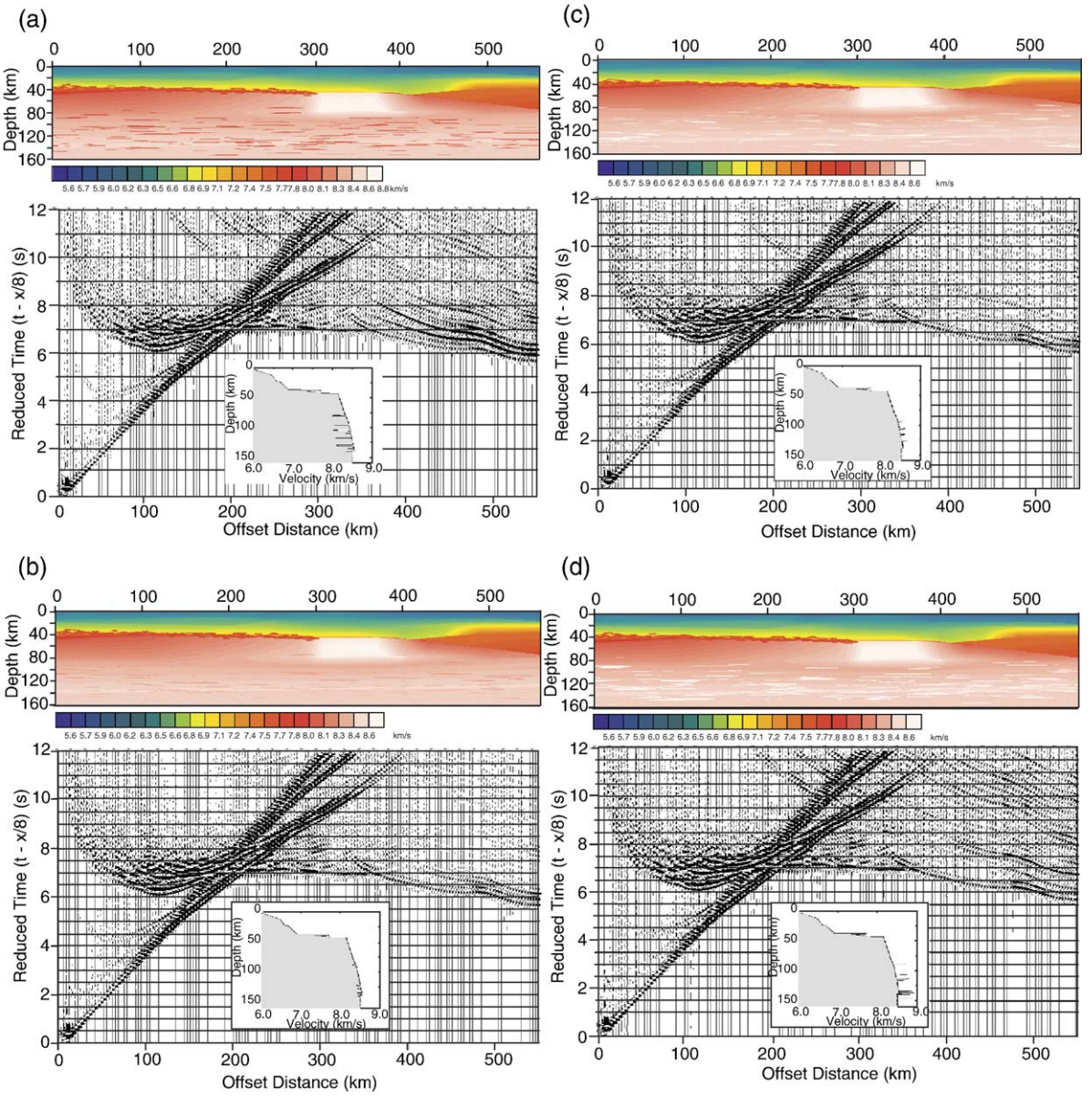

Fig. 11. Pseudo-spectral modelling of velocity contrasts within upper mantle heterogeneous bodies based on seismic record ThoRE 201. The structure of the models (upper portion of each part of the figure) is determined by ray-theoretical travel-time modelling. Heterogeneities in the upper mantle are added by the addition of stochastically defined elliptical bodies. See Table 3 for details. A representative 1-D P-wave velocity model is plotted for each model. (a) Velocities of heterogeneities are ~0.3 km/s less than the surrounding mantle. (b) Velocities are ~0.1 km/s less. (c) Velocities are ~0.1 km/s more than the surrounding mantle. (d) Velocities are ~0.3 km/s greater.

onset or end. This evolution of the Pn_2P with offset is probably related to a change in the way the seismic energy returns from the inhomogeneities. At offsets less than ~1000 km, the Pn_2P phase mainly consists of arrivals that are near-critical-angle reflections. At distances greater than ~1000 km, the first arrival wave-front travels nearly horizontally in the modelled depth range. Since the energy travels parallel to the longest axes of the inhomogeneities, the waves recorded at the surface for these offsets are not reflected arrivals but scattered phases (Aki and Richards, 1980). Differences in the arrival times of Pn_2P at offsets beyond 1000 km between the two models indicate that the Pn_2P phase advances or lags behind the Pn, depending on the velocity of the inhomogeneities. Consequently, the upper mantle heterogeneous layer acts as a wave-guide beyond offsets of ~1000 km.

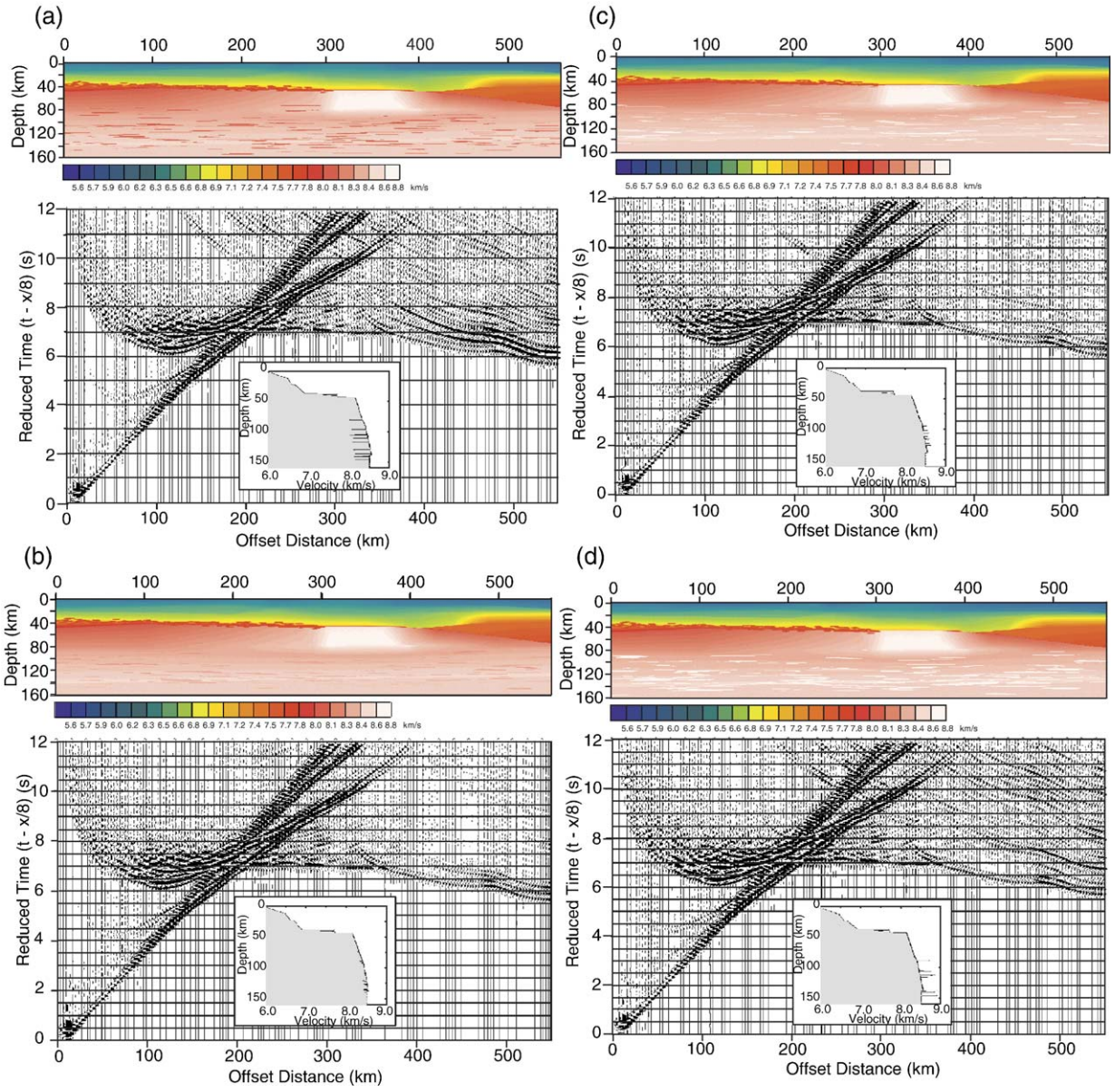

Fig. 12. Pseudo-spectral modelling of heterogeneous body dimensions within the upper mantle based on seismic record ThoRE 201. The structure of the models (upper portion of each part of the figure) is determined by ray-theoretical travel-time modelling. Heterogeneities in the upper mantle are added by the addition of stochastically defined elliptical bodies. See Table 3 for details. A representative 1-D P-wave velocity model is plotted for each model. Average dimensions of heterogeneities are: (a) 40.0×0.2 km, (b) 10.0×0.2 km, (c) 5.0×0.2 km, and (d) 2.5×0.2 km.

The calculated synthetic refraction shot records (Fig. 11a and d) show that inhomogeneities, both with lower or higher than average velocity, generate a nearly identical Pn_2P phase in a typical refraction offset range (300 to 800 km). Therefore, it is not possible to determine the velocity of the inhomogeneities from the refraction shot records. However, at greater offsets, the Pn_2P shows significant variation in arrival time (Fig. 14), which appears to depend on the velocity of the inhomogeneities. The Pn_2P phase in the Deep Probe data (Fig. 8a), with offsets as great as 1350 km, are similar in character to those modelled with heterogeneities with a lower than average velocity (Fig. 14b).

7.1. Inferences from the modelling

The Alberta Basement and Trans-Hudson Orogen transects add to a growing list of regions where there is

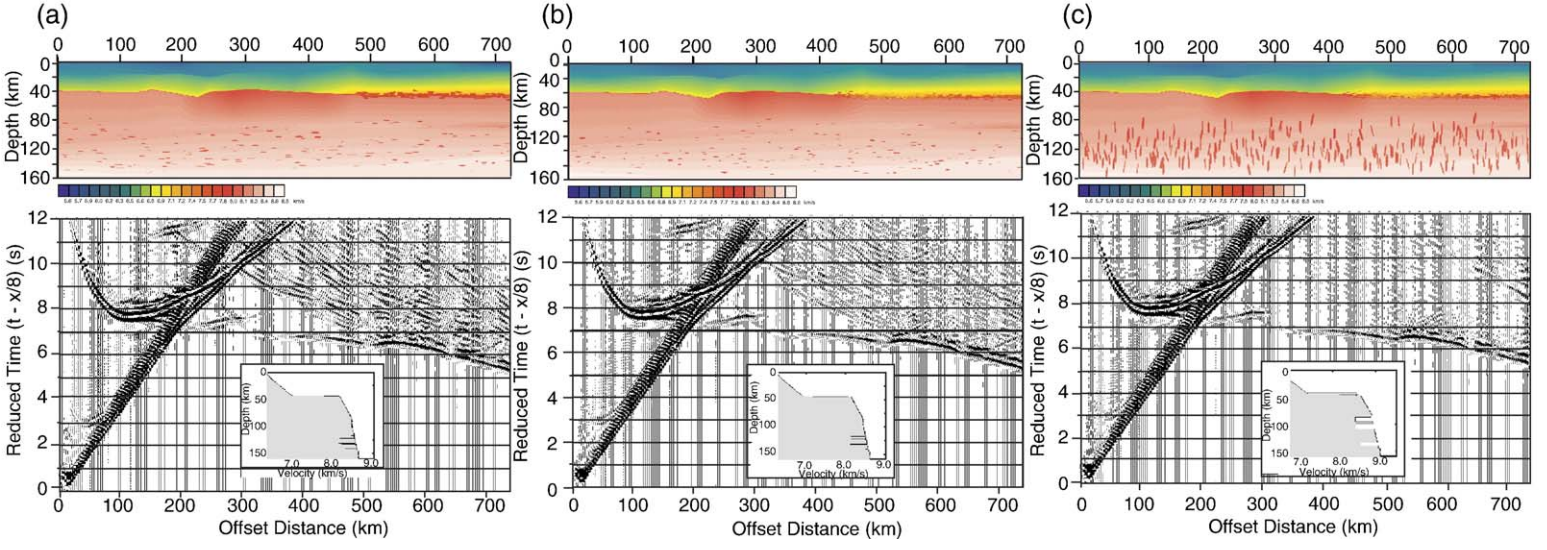

Fig. 13. Pseudo-spectral modelling of heterogeneous body dimensions within upper mantle based on seismic record ThoRE 101. The structure of the models (upper portion of each part of the figure) is determined by ray-theoretical travel-time modelling. Heterogeneities in the upper mantle are added by the addition of stochastically defined elliptical bodies. See Table 3 for details. A representative 1-D P-wave velocity model is plotted for each model. Average dimensions of heterogeneities are: (a) 5.0 × 0.2 km, (b) 3.5 × 0.2 km, and (c) 1.5 × 20.0 km.

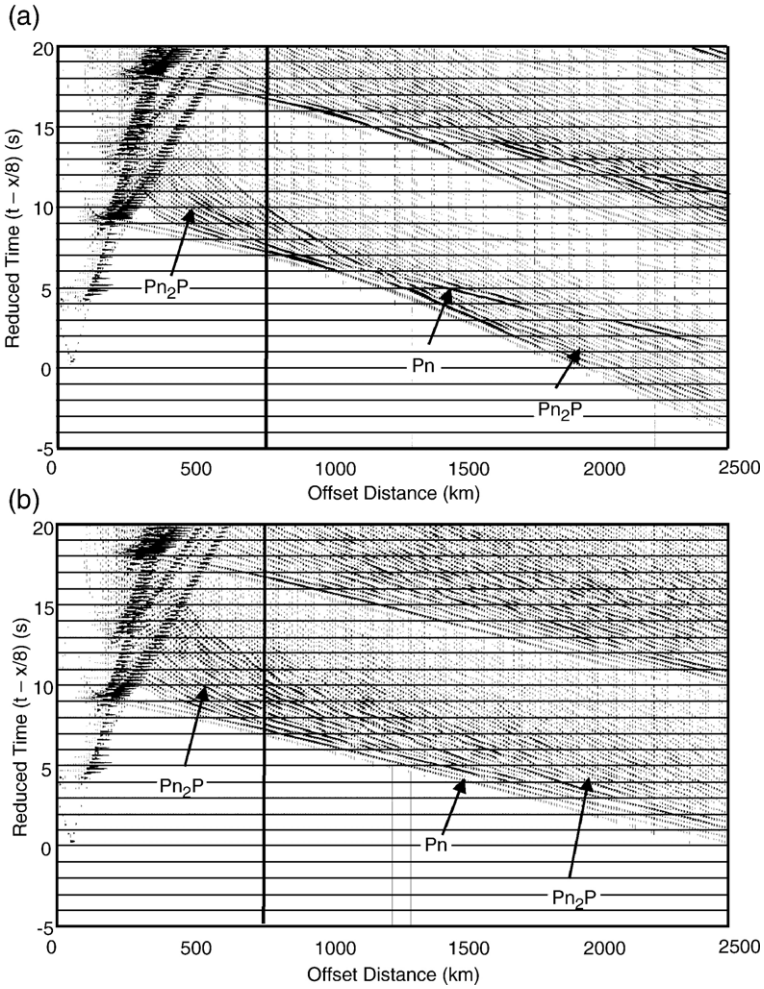

Fig. 14. Nature of Pn_2P at teleseismic distances. (a) Mantle structures are the same as for Fig. 11d. (b) Mantle structures as for Fig. 11a. The thick vertical line indicates the maximum offset (750 km) of the refraction observations. Note, that at offsets less than 750 km the two records are nearly identical. At greater offsets (> 1000 km), the apparent velocity of the Pn_2P is defined by the velocity of the inhomogeneities. This evolution indicates a change in the way the energy returns to the surface. The secondary phases that arrive ~10 s behind the first arrival are multiples generated in the crust.

strong evidence for a seismically transparent uppermost mantle (i.e., the region between the Moho and the layer of upper mantle heterogeneities modelled here.) Even though this transparent zone is characterised by little reflectivity, a significant variation in bulk velocity is observed. These upper mantle velocity variations often cannot be correlated in first order fashion to known geological domains; however, there do appear to be links between modelled upper mantle features and the overlying crust. For example, the high velocity zone imaged in the uppermost mantle on THoRE profile R2 (Figs. 11 and 12) is interpreted in three dimensions to correspond to a region of strong anisotropy (8.6 km/s NNW/SSE and 8.1 km/s ENE/WSW) (Németh et al., 2005). The same feature is interpreted along THoRE profile R3. Németh et al. (2005) attribute the localised area of uppermost mantle seismic anisotropy to be associated with tectonic deformation following the last collisional stage of the orogen's development. In the case of the Deep Probe/SAREX data, the upper mantle dipping reflectors appear to correspond to domain boundaries in the overlying crust. The connections between these upper mantle features and the overlying crust suggest that these depths of the upper mantle constitute a stable, long-lived component of the continental lithosphere.

The thickness and physical characteristics of the heterogeneous upper mantle layers of the Alberta Basement and Trans-Hudson Orogen transects are remarkably similar. For the Alberta Basement, the preferred model invoked elliptical inhomogeneities with average lengths of 36 km, thicknesses of

0.72 km, and velocity contrasts of ~−0.3 km/s between depths of 90 and 140 km. For the Trans-Hudson Orogen, the preferred model contained similar elliptical inhomogeneities with average lengths of 20 to 40 km, thicknesses of 0.2 km and velocity contrasts of −0.3 to −0.4 km/s between depths of 78 and 150 km. For example, this velocity contrast is consistent with determinations of velocity for a 1% melt fraction in the upper mantle (Hammond and Humphreys, 2000). Similarly, the variations may represent upper mantle lithological differences such as the contrast between peridotite and eclogite (Warner et al., 1996). In either case, the variations could be inherited from intrinsic anisotropy in an earlier rheological or petrological state.

The consistency of the layer beneath two different cratonic provinces, the Archaean of the Alberta Basement and the Proterozoic of the Trans-Hudson Orogen, suggests that the layer's physical nature is due to depth dependent rheological or thermal characteristics rather than petrological characteristics of a particular lithospheric domain. If the Trans-Hudson Orogen were considered alone, then classifying the layer as part of the lithosphere or asthenosphere could be problematic. However, the dipping reflectors in the Deep Probe model from southern Alberta extend down into the heterogeneous layer suggesting that the layer must have been in place at the time of the processes that led to the dipping events. If these dipping events are features related to Proterozoic or older subduction, then the heterogeneous layer must be a stable part of the lithosphere for at least as long as the dipping structures have been present.

The observations made in these R/WAR surveys are band limited between roughly 0.5 and 8.0 Hz. Passive seismic analysis techniques such as teleseismic receiver functions and shear-wave splitting analyses have the potential to image the heterogeneous layer in different ways using lower frequencies. Shear wave splitting results from the Alberta Basement transect show fast directions striking SW–NE (Shragge et al., 2002). This is consistent with the orientation of low-velocity cigar-shaped heterogeneities within the Trans-Hudson Orogen. The resolution of the Alberta teleseismic data is not sufficient to detect an overall decrease in velocity corresponding to the heterogeneous layer modelled here; however, such observations are being made in the upper mantle beneath other Precambrian cratons (e.g., Superior province, Frederiksen et al., 2004).

8. Conclusions

The major result of this work is the confirmation and partial characterisation of a widespread heterogeneous layer in the 80–150 km depth range of the upper mantle beneath western Canada. The layer is independent of the overlying crust and is in agreement with similar models developed for the Siberian and Baltic Shields. At the scale of these observations, the heterogeneous layer can be parameterized by a stochastic distribution of elliptical bodies with average lengths of 20–40 km thicknesses of 0.20–0.72 km and velocity contrasts of −0.3 to −0.4 km/s from the background velocity of the upper mantle. Observations of orthogonal profiles in the Trans-Hudson Orogen transect suggest that the heterogeneous bodies are elongated in the north–south direction and shortened in the east–west direction resulting in cigar-shaped anomalies. This is consistent with teleseismic shear-wave splitting analyses conducted in the Alberta Basement transect (Shragge et al., 2002).

Even though the heterogeneous layer is widespread beneath a range of crustal domains, we prefer to consider the layer as part of the lithosphere. The structure and physical origin of the upper mantle heterogeneous layer is usually explained by some process that is either the cause of lateral flow in the upper mantle (e.g., Bostock, 1998) or may facilitate lateral flow in the upper mantle (e.g., Thybo and Perchuc, 1997). This leads to the layer being intrinsically involved with the rheological differentiation of the lithosphere and asthenosphere—either as the lowest layer of the lithosphere or the upper layer of the asthenosphere. However, is this rheological scenario current or just a snapshot from the Precambrian? The upper mantle dipping reflectors modelled in the Alberta Basement transect support the latter conclusion. Thus, the heterogeneous layer is interpreted to be the lowest layer of the lithosphere, consistent with the relatively thick lithosphere inferred by Shragge et al. (2002) from their passive teleseismic study.

Deep lithospheric studies such as this provide potential for overlap between passive-source teleseismic and controlled-source R/WAR techniques. This is especially important in this case where the base of the heterogeneous layer is determined by modelling the termination of the Pn_2P phase reflections. Models produced here are built on the assumption that the heterogeneous bodies cease to occur at a depth of ~150 km. However, insignificant signal penetration is another explanation for the termination—or fading out—of observed reflections in the seismic data.

Acknowledgements

We thank Alan Levander and Lars Nielsen for their insightful and rigorous reviews. Lithoprobe Publication Number 1410.

References

Aki, K., Richards, P.G., 1980. Quantitative Seismology. W.H. Freeman and Co.

Alford, R.M., Kelly, K.R., Boore, D.M., 1974. Accuracy of finite-difference modeling of the acoustic wave equation. Geophysics 39 (6), 834–842.

Allègre, C.J., Turcotte, D.L., 1986. Implications of a two-component marble-cake mantle. Nature 323 (6084), 123–127.

BABEL Working Group, 1990. Evidence for early Proterozoic plate tectonics from seismic reflection profiles in the Baltic shield. Nature 348, 34–38.

BABEL Working Group, 1993. Integrated seismic studies of the Baltic Shield using data in the Gulf of Bothnia region. Geophysical Journal International 112, 305–324.

Bath, M., 1966. Propagation of Sn and Pn to teleseismic distances. Pure and Applied Geophysics 64, 19–30.

Bath, M., 1967. Observations of teleseismic Pn phases. Pure and Applied Geophysics 66 (1), 30–36.

Bostock, M.G., 1998. Mantle stratigraphy and evolution of the Slave province. Journal of Geophysical Research 103, 21,183–21,200.

Cerveny, V., Molotkov, I.A., Psenvcik, I., 1977. Ray Method in Seismology. Univerzita Karlova, Prague.

Chapman, C.H., 1985. Ray theory and its extensions: WKBJ and Maslov seismograms. Journal of Geophysics 58, 27–43.

Clowes, R.M., et al., 1999. Canada's LITHOPROBE Project (Collaborative, multidisciplinary geoscience research leads to new understanding of continental evolution). Episodes 22 (1), 3–20.

Clowes, R.M., Buriyank, M.J.A., Gorman, A.R., Kanasewich, E.R., 2002. Crustal velocity structure from SAREX, the Southern Alberta Refraction Experiment. Canadian Journal of Earth Sciences 39 (3), 351–373.

Crossley, D.J., Jensen, O.G., 1989. Fractal velocity models in refraction seismology. Pure and Applied Geophysics 51, 54–66.

Deep Probe Working Group, 1998. Probing the depths of western North America: contrasting Archean and Proterozoic lithosphere with controlled source seismology. GSA Today 8 (7), 1–5.

Egorkin, A.V., Pavlenkova, N.I., 1981. Studies of mantle structure of USSR territory on long-range seismic profiles. Physics of the Earth and Planetary Interiors 25, 12–26.

Egorkin, A.V., Zuganov, S.K., Pavlenkova, N.I., Chernyshov, N.M., 1987. Results of lithospheric studies from long-range profiles in Siberia. Tectonophysics 140, 29–47.

EUGENO-S Working Group, 1988. Crustal structure and tectonic evolution of the transition between the Baltic Shield and North German Caledonides (the EUGENO-S project). Tectonophysics 294, 43–55.

Fernandez Viejo, G., Clowes, R.M., Amor, J.R., 1999. Imaging the lithospheric mantle in northwestern Canada with seismic wide-angle reflections. Geophysical Research Letters 26 (18), 2809–2812.

Frederiksen, A.W., Miong, S., Eaton, D.W., 2004. Mantle fabric beneath Ontario: results from the CNSN, FEDNOR and PLOARIS Arrays. Eos, Transactions, American Geophysical Union 85 (47) (Abstract T33A-1326).

Fuchs, K., Schulz, K., 1976. Tunneling of low-frequency waves through subcrustal lithosphere. Journal of Geophysics-Zeitschrift fur Geophysik 42 (3), 175–190.

Gazdag, J., 1982. Modelling of the acoustic wave equation with transform methods. Geophysics 46, 854–859.

Gorman, A.R., 2000. Deep Probe: Investigating the Lithosphere of Western North America with Refraction Seismology. PhD Thesis, University of British Columbia, Vancouver. 230 pp.

Gorman, A.R., et al., 2002. Deep probe: imaging the roots of western North America. Canadian Journal of Earth Sciences 39 (3), 375–398.

Guggisberg, B., Berthelsen, A., 1987. A two-dimensional velocity model for the lithosphere beneath the Baltic Shield and its possible tectonic significance. Terra Cognita 7, 631–638.

Hammond, W.C., Humphreys, E.D., 2000. Upper mantle seismic wave velocity: effects of realistic partial melt geometries. Journal of Geophysical Research 105 (B5), 10,975–10,986.

Kelly, K.R., Ward, R.W., Treitel, S., Alford, R.M., 1976. Synthetic seismograms: a finite difference approach. Geophysics 41 (1), 2–27.

Kosloff, D.D., Baysal, E., 1982. Forward modelling by a Fourier method. Geophysics 47, 1402–1412.

Levander, A.R., 1989. In: James, D.E. (Ed.), Finite Difference Forward Modelling in SeismologyEncyclopedia of Solid Earth Geophysics, vol. 16, pp. 410–431.

Levander, A., Holliger, K., 1992. Small-scale heterogeneity and large-scale structure of the continental crust. Journal of Geophysical Research 94, 17749–17765.

Levander, A., et al., 1994. The crust as a heterogeneous "optical" medium, or "crocodiles in the mist". Tectonophysics 232 (1–4), 281–297.

Meibom, A., Anderson, D.L., 2003. The statistical upper mantle assemblage. Earth and Planetary Science Letters 217 (1–2), 123–139.

Menke, W.H., Richards, P.G., 1980. Crust–mantle whispering gallery phases: a deterministic model of teleseismic Pn wave propagation. Journal of Geophysical Research 85 (B10), 5416–5422.

Morozov, I.B., 2001. Comment on "High-frequency wave propagation in the uppermost mantle" by T. Ryberg and F. Wenzel. Journal of Geophysical Research 106 (B12), 30,715.

Morozov, I.B., Smithson, S.B., 2000. Coda of long-range arrivals from nuclear explosions. Bulletin of the Seismological Society of America 90, 929–939.

Morozov, I.B., Morozova, E.A., Smithson, S.B., Solodilov, L.N., 1998. On the nature of the teleseismic Pn Phase observed on the ultralong-range profile Quartz, Russia. Bulletin of the Seismological Society of America 88 (1), 62–73.

Nielsen, L., Thybo, H., 2003. The origin of teleseismic Pn waves: multiple crustal scattering of upper mantle whispering gallery phases. Journal of Geophysical Research 108 (B10), 2460. doi:10.1029/2003JB002487.

Nielsen, L., Thybo, H., Egorkin, A.V., 2002. Implications of seismic scattering below the 8° discontinuity along PNE profile Kraton. Tectonophysics 358, 135–150.

Nielsen, L., Thybo, H., Levander, A., Solodilov, L.N., 2003. Origin of upper-mantle seismic scattering—evidence from Russian peaceful nuclear explosion data. Geophysical Journal International 154, 196–204.

Németh, B., 1999. Structure of the Lithosphere Within the Trans-Hudson Orogen (Results of the 1993 Lithoprobe Trans-Hudson Refraction Experiment). University of Saskatchewan, Saskatoon. 143 pp.

Németh, B., Hajnal, Z., 1998. Structure of the lithospheric mantle beneath the Trans-Hudson Orogen, Canada. Tectonophysics 288, 1–4.

Németh, B., Hajnal, Z., Lucas, S.B., 1996. Moho signature from wide-angle reflections: preliminary results of the 1993 Trans-Hudson Orogen refraction experiment. Tectonophysics 264, 111–121.

Németh, B., Clowes, R.M., Hajnal, Z., 2005. Lithospheric structure of the Trans-Hudson Orogen from seismic refraction/wide-angle reflection studies. Canadian Journal of Earth Sciences 42, 435–456.

Pavlenkova, N.I., 1996. General features of the uppermost mantle stratification from long-range seismic profiles. Tectonophysics 264, 261–278.

Perchuc, E., Thybo, H., 1996. A new model of upper mantle P-wave velocity below the Baltic Shield: indication of partial melt in the 95 to 160 km depth range. Tectonophysics 253, 227–245.

Reston, T.J., 1987. Spatial interference, reflection character and structure of the lower crust under extension: results from 2-D seismic modelling. Annales Geophysica 5B, 339–348.

Robertsson, J.O.A., Blanch, J.O., Symes, W.W., 1994. Viscoelastic finite-difference modeling. Geophysics 59, 1444–1456 (September 1994).

Ryberg, T., Fuchs, K., Egorkin, A.V., Solodilov, L.N., 1995. Observation of high-frequency teleseismic Pn on the long-range Quartz profile across northern Eurasia. Journal of Geophysical Research 100 (B9), 18,151–18,163.

Ryberg, T., et al., 1996. Two-dimensional velocity structure beneath Northern Eurasia derived from the super long-range seismic profile Quartz. Bulletin of the Seismological Society of America 857–867.

Shragge, J., Bostock, M.G., Bank, C.-G., Ellis, R.M., 2002. Integrated teleseismic studies of the southern Alberta upper mantle. Canadian Journal of Earth Science 39 (3), 399–411.

Thybo, H., Perchuc, E., 1997. The seismic 8° discontinuity and partial melting in continental mantle. Science 275, 1626–1629.

Tittgemeyer, M., Wenzel, F., Fuchs, K., Ryberg, T., 1996. Wave propagation in a multiple-scattering upper mantle—observations and modelling. Geophysical Journal International 127, 492–502.

Tittgemeyer, M., Wenzel, F., Ryberg, T., Fuchs, K., 1999. Scales of heterogeneities in the continental crust and upper mantle. Pure and Applied Geophysics 156, 29–52.

Tittgemeyer, M., Wenzel, F., Fuchs, K., 2000. On the nature of Pn. Journal of Geophysical Research 105, 16,173–16,180.

Villeneuve, M.E., et al., 1993. Tectonic subdivision and U–Pb geochronology of the crystalline basement of the Alberta Basin, Western Canada. GSC Bulletin 447 (86 pp.).

Warner, M., et al., 1996. Seismic reflections from the mantle represent relict subduction zones within the continental lithosphere. Geology 24, 39–42.

Zelt, C.A., Smith, R.B., 1992. Seismic traveltime inversion for 2-D crustal velocity structure. Geophysical Journal International 108, 16–34.